

Simulation of mirages

W. H. Lehn and W. Friesen

A mirage is seen when atmospheric refraction distorts or displaces an image. We describe a mirage simulator that uses digital imaging equipment to generate mirage images from normal photographs. The simulation program relocates horizontal image lines into positions that they appear to occupy, according to rays traced from observer to object. Image-brightness adjustments are not required; we show that, while the atmosphere can change the size or shape of an object, it does not change its apparent brightness. The realistic quality of the computed images makes this simulator a useful tool in mirage analysis.

I. Introduction

The term mirage is used for images that are distorted or displaced by a refracting atmosphere. The refractive ability of air depends on the gradient of its refractive index, which in turn depends mainly on the temperature gradient.¹ Thus a mirage can be computed by tracing rays through an atmosphere of known temperature distribution (the forward problem). Alternatively, the knowledge of the true shape of an object, together with its mirage image, may permit reconstruction of the temperature distribution (the inverse problem). Work on both problems is greatly facilitated if a realistic mirage image can be displayed.

In this paper we describe the development of a mirage simulator that produces monochrome continuous tone images calculated from digitized source photographs.² The approach is distinct from the work of Berger *et al.*³ in that it does not require the creation of a three-dimensional computer graphics model of the object—rather, it uses original photographs of real objects to provide a far higher degree of realism.

The imaging properties of a given atmosphere can be graphically summarized in two distinct forms. Each of these requires the tracing of a bundle of rays out from the observer's eye, and each is a representation of the apparent height of object points in the field of view. Apparent height is computed by straight-line backprojection of rays entering the observer's eye.

One form is the image space,⁴ which shows the

apparent heights of surfaces of constant elevation. The image-space concept is most useful for estimating images of objects that possess considerable longitudinal extent, i.e., varying distance from the observer. The second form, which carries the smaller computational burden, is the transfer characteristic.⁵ This is a graph of apparent versus actual elevation of object points at a single specific distance from the observer, i.e., it is a cross section of the image space at a fixed distance. This form is more convenient and is sufficiently accurate if the object's longitudinal extent is small relative to its distance from the observer. A large proportion of practical mirages falls into this category.

Detailed image construction is laborious with both representations; typically, the points on a line drawing of the object are individually mapped into new apparent positions and joined by straight lines to create a line drawing of the image.⁶ Entry of object data is slow; either individual coordinates are entered by hand or the object can be traced on a digitizing tablet. Because the computed image is still only a line drawing, it is not entirely satisfactory. Certainly it is not convincingly realistic when compared with a direct photograph of a mirage.

II. Image Calculation

Commonly available image-processing equipment, consisting of a camera, a frame grabber, and a personal computer, is sufficient to generate realistic mirage simulations. The equipment used in this work consisted of a PCVision 640 × 480 pixel frame grabber (Imaging Technology, Inc.), installed in an IBM PC AT-compatible personal computer. Indeed, once the original image is digitized and stored, a VGA monitor is adequate to display the results. Versions of the software have been written in both C and PASCAL.

The starting point is an undistorted image of the

The authors are with the Department of Electrical and Computer Engineering, University of Manitoba, Winnipeg R3T 2N2, Canada.

Received 13 March 1991.

0003-6935/92/091267-07\$05.00/0.

© 1992 Optical Society of America.

object. This may be obtained from the same station from which the mirage was observed, as long as one is certain that no mirage is present (this is not a trivial problem in polar regions). Alternatively, a photograph made at closer range may be used, provided that its perspective and line of sight are consistent with the mirage photograph geometry.

The method selected for the simulation is based on the transfer characteristic (TC) approach. The TC may be generated by tracing a bundle of rays through any suitable atmospheric model; or it may, for experimental purposes, be arbitrarily created. The quality of the result will clearly depend on the ray-tracing algorithm in use. Such algorithms are discussed elsewhere.^{7,8} Thus, for example, the spherical shell model that uses a continuous temperature function and accounts for pressure variation with elevation will produce better results than a process³ that does neither of these.

When the undistorted photograph is digitized, a vertical distance scale is imposed on it. The actual elevations of two selected pixels must be entered by means of a cursor or a horizontal reference line. These pixels are normally the highest object point on the horizon. The computer thus knows the object

scale (meters per pixel) and uses the same scale to display the calculated image.

The image is calculated from the TC, which is entered as an array of data points. Figure 1 shows the results of a typical calculation; the temperature profile determines the shape of a ray bundle, from which the TC is extracted. Because the TC is frequently multiple valued in its abscissa (z_{obj}) but always single valued in its ordinate (z_{app}), the image calculation procedure scans the TC upward along the ordinate, in a step size equal to the object scale. For each step in z_{app} , the corresponding object elevation is computed by linear interpolation and quantized to the same step size. The results are stored in a one-dimensional array as follows:

The index number of each element is equal to the row number of the mirage image to be displayed, while the value of each element is the row number of the original image that is to be displayed in this location. Thus the whole operation is simply a relocation of object pixel rows into image rows, as dictated by the TC.

Adjustment of pixel brightness is not required in the creation of the mirage image; we show in Appendix A that apparent brightness does not change when

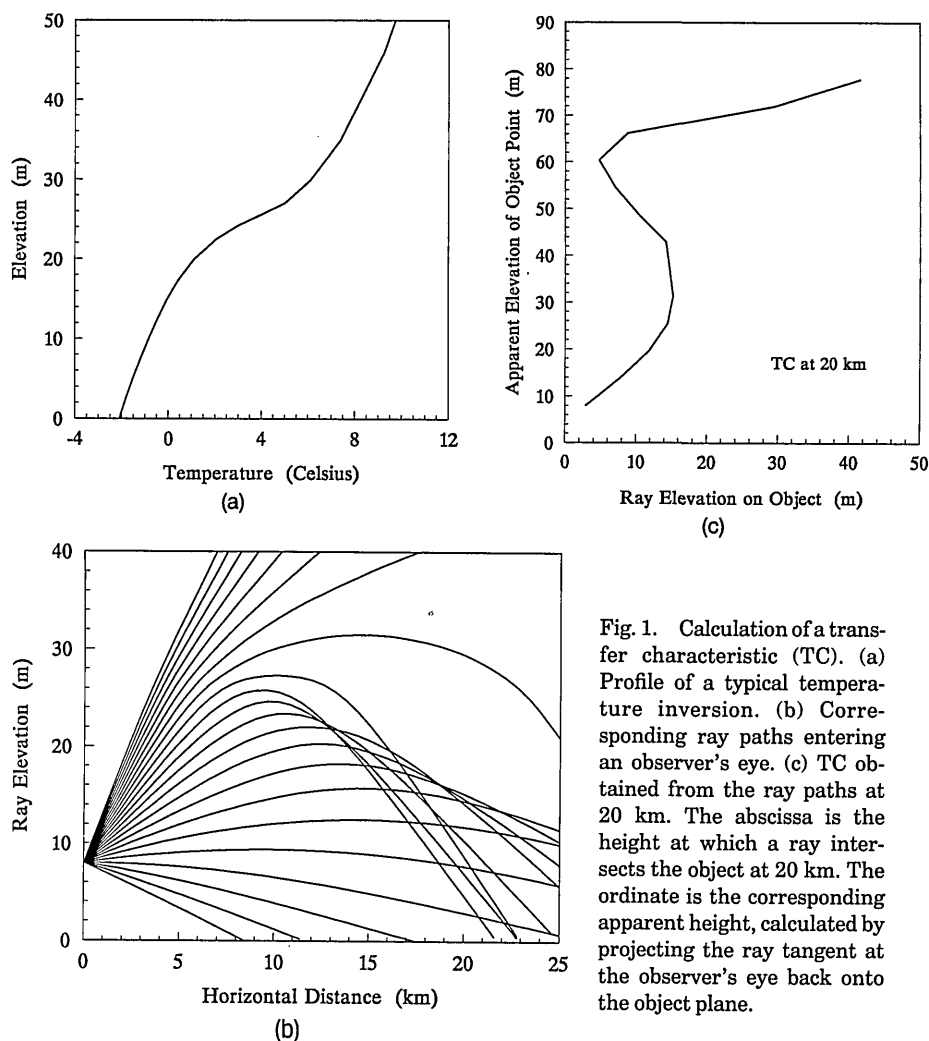


Fig. 1. Calculation of a transfer characteristic (TC). (a) Profile of a typical temperature inversion. (b) Corresponding ray paths entering an observer's eye. (c) TC obtained from the ray paths at 20 km. The abscissa is the height at which a ray intersects the object at 20 km. The ordinate is the corresponding apparent height, calculated by projecting the ray tangent at the observer's eye back onto the object plane.

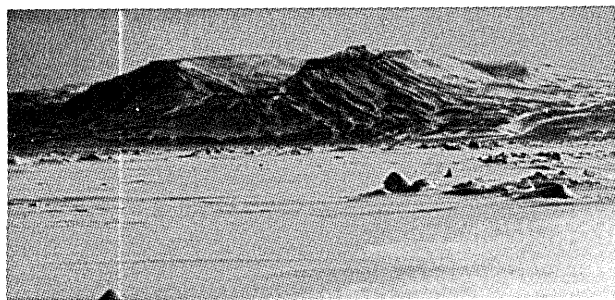
the atmosphere distorts a normal image into a mirage. This result is consistent with our photographic observations; clearly defined mirage images have shown no anomalous brightness distributions.

The calculated image will occupy fixed limits on the screen, which are determined by the lowest and highest ordinate values in the TC [Fig. 1(c)]. If this image does not fill the screen, further steps are taken. The lower part of the screen is filled with the original foreground. This normally produces minimal errors because rays striking the ground without propagating to the object generally have short ranges for which refractive distortions tend to be minimal. The upper part of the screen is filled with the sky image from the original object; because sky is generally featureless, this also produces no disturbing effects. In practice, as the examples in Section III show, these sky and foreground additions contribute to realistic images.

III. Examples

The following examples demonstrate the capability of the mirage simulator to generate realistic equivalents of actual observations and to explore new possibilities that might be observed:

1. The image pair in Fig. 2 was obtained at Resolute Bay, Northwest Territories, Canada. The elevation of the highest peak is 340 m (map data). The corresponding TC is deduced by measuring the elevations of corresponding points in Fig. 2(a) (actual elevation) and Fig. 2(b) (apparent elevation). The result, after some fine tuning based on image comparison, is shown in Fig. 3. The calculated mirage image (Fig. 4) as photographed on the display monitor



(a)



(b)

Fig. 2. (a) Normal view of mountains on Somerset Island, Northwest Territories, Canada, on 31 May 1987. (b) Mirage of the same mountains photographed from Resolute Bay, Northwest Territories, at a distance of ~75 km on 7 June 1985.

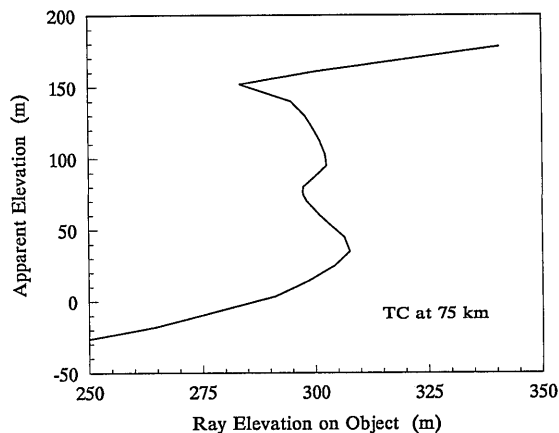


Fig. 3. TC deduced from the photographs of Fig. 2.

provides a realistic and quite accurate representation of the actual mirage photograph. Small differences may be attributed to the assumptions made at the outset: that the target object occupies a single plane and that the atmosphere is laterally homogeneous.

2. Figure 5(a) shows a line of hills bordering the Beaufort Sea, at Tuktoyaktuk, Northwest Territories, Canada; Figs. 5(b) and 5(c) show superior and inferior mirages, respectively. The two corresponding TC curves (Fig. 6) generate the simulated versions of Fig. 7. Again, real-appearing images are seen on the monitor. A staircase effect is visible in Fig. 7(a) because (i) the original image has small vertical extent and (ii) the vertical magnification of the mirage is large. In the high-magnification zone each original image line is repeated several times in the mirage image, resulting in the stepped appearance.

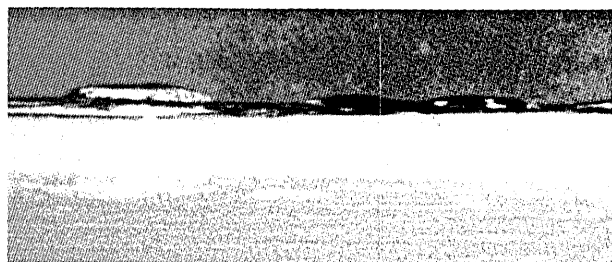
3. The mirage simulator can be used to test new possibilities. For example, mirages provide a good scientific explanation^{9,10} for frequently reported sightings of lake and sea monsters.¹¹ A mirage can distort any ordinary object into unrecognizable shape, as illustrated in Fig. 8. Here a group of walrus photographs in the wild by Fred Bruemmer¹² takes on monstrous proportions when processed by the TC of Fig. 8(c).

IV. Conclusions

This approach to simulating mirage images produces realistic results. The simulation is designed for a



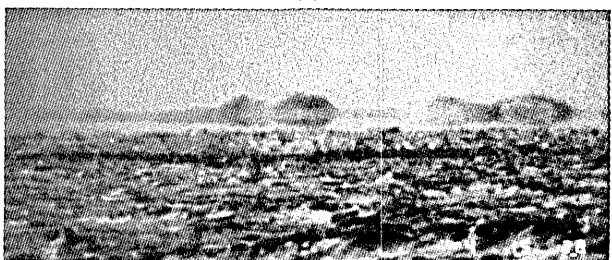
Fig. 4. Mirage simulation obtained by applying the TC of Fig. 3 to the undistorted image of Fig. 2(a).



(a)



(b)



(c)

Fig. 5. (a) Undistorted photograph of Naparotalik Spit, taken from Tuktoyaktuk, Northwest Territories, on 26 May 1979 (the distance is 13.2 km). The height of the domed hill at the left is 11.2 m. (b) Superior mirage of the same hills, observed on 16 May 1979. (c) Inferior mirage, 4 May 1983.

single-object distance in atmospheres that may vary along, but not across, the line of sight. It is a sensitive accuracy test for TC's determined from image measurements. Its main usefulness to mirage analysis lies in the evaluation of atmospheric models. In most

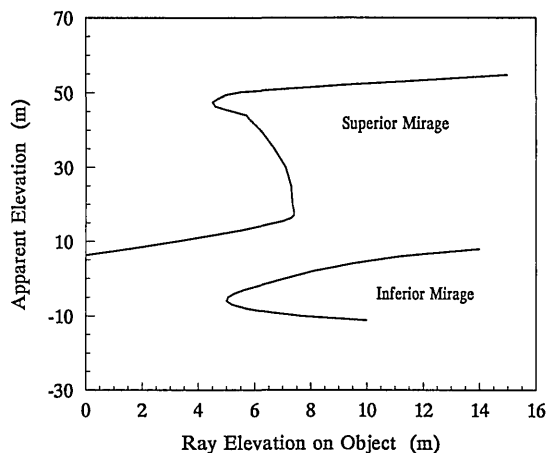
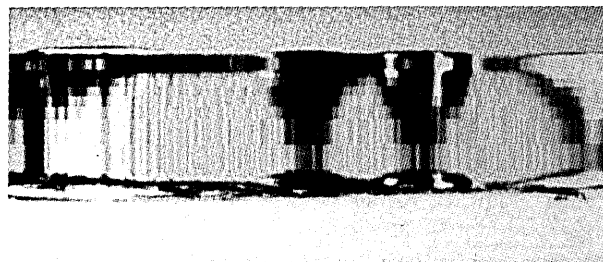
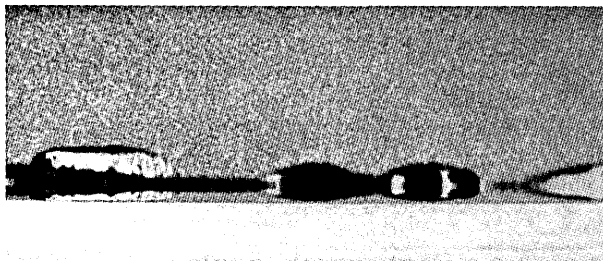


Fig. 6. TC curves deduced from Fig. 5.



(a)



(b)

Fig. 7. Mirage simulations obtained by applying the TC's of Fig. 6 to Fig. 5(a): (a) superior mirage, (b) inferior mirage.

cases the determining factor in the assessment of model validity is the degree to which model images agree with field observations.

Appendix A

We show that in the spherically symmetric atmosphere the brightness distribution in a mirage image is the same as that of the normal image. First we obtain a relation between the angle subtended by a unit area looking backward and that looking forward along the same ray; then we use this result to compare the irradiance of a mirage image with that of its undistorted counterpart.

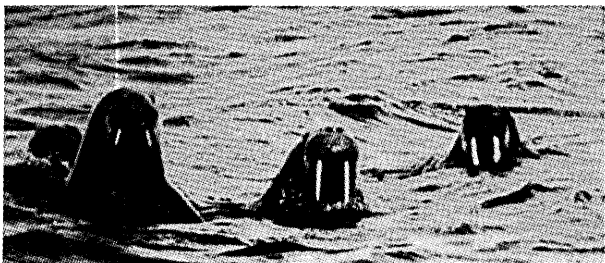
The equation of the ray path is given in standard references.^{14,15} To review briefly, we use polar coordinates r, ϕ with the origin at the Earth's center (Fig. 9). The refractive index n is a function of r only. Each ray is contained in a plane that includes the origin. Along a given ray the quantity $nr \sin \theta = k$ is invariant, where θ is the zenith angle of the ray. From the ray invariant the equation of the ray path itself can be found:

$$\phi = \int_{\phi_A}^{\phi_B} d\phi = \int_{r_A}^{r_B} f(r, n, k) dr, \quad (A1)$$

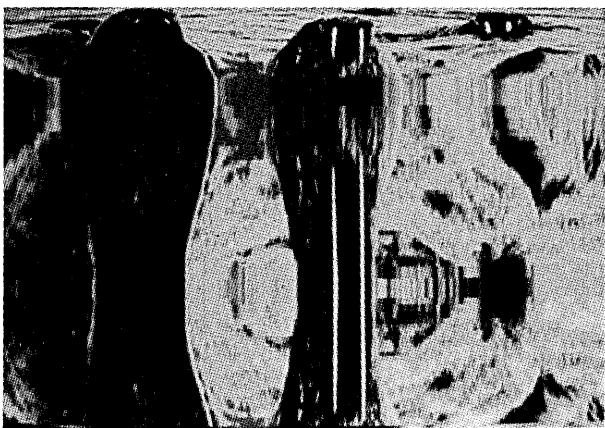
where $f(r, n, k) = k/r(n^2 r^2 - k^2)^{1/2}$.

Begin with the observer at A (Fig. 9) and calculate the vertical angle subtended by a small radial displacement at B, i.e., let r_B increase by a small amount ϵ , and find the resulting change $d\theta$ in θ . Since the ray AB and the new ray to $r_B + \epsilon$ share the same ϕ value, the path integrals can be equated:

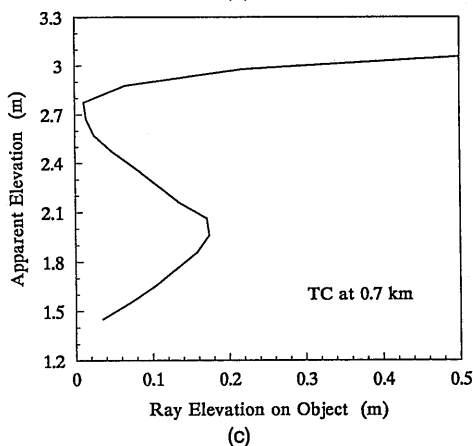
$$\int_{r_A}^{r_B} f(r, n, k) dr = \int_{r_A}^{r_B + \epsilon} f(r, n, k') dr, \quad (A2)$$



(a)



(b)



(c)

Fig. 8. (a) Walrus in their natural environment, photographed by F. Bruemmer.¹² (b) The walrus take on the aspect of sea monsters, much as described in the 13th Century book, *King's Mirror*.¹³ (c) TC required to create the mirage.

where the new ray has a new invariant $k' = k + dk$. Both k and k' have the same n_A and r_A values; they differ only because of $d\theta$: $dk = n_A r_A \cos \theta d\theta$. Also,

$$f(r, n, k') = f(r, n, k) + \frac{\partial f}{\partial k} dk, \quad (\text{A3})$$

where

$$\frac{\partial f}{\partial k} = \frac{n^2 r}{(n^2 r^2 - k^2)^{3/2}}. \quad (\text{A4})$$

Use Eqs. (A3) and (A4) in Eq. (A2) and split the

right-hand integral into two:

$$\int_{r_A}^{r_B} f(r, n, k) dr = \int_{r_A}^{r_B} \left[f(r, n, k) + \frac{\partial f}{\partial k} dk \right] dr + \int_{r_B}^{r_B+\epsilon} \left[f(r, n, k) + \frac{\partial f}{\partial k} dk \right] dr. \quad (\text{A5})$$

Perform the obvious cancellation and ignore terms of second order to obtain the angle subtended by ϵ at A:

$$d\theta = - \frac{\epsilon \tan \theta}{I r_B (n_B^2 r_B^2 - k^2)^{1/2}}, \quad (\text{A6})$$

where

$$I = \int_{r_A}^{r_B} \frac{n^2 r dr}{(n^2 r^2 - k^2)^{3/2}}. \quad (\text{A7})$$

We now reverse the ray to obtain the angle subtended by a height ϵ at A as seen by an observer at B. Interchange the subscripts A and B. Let α be the zenith angle of the ray BA at B (note that $\alpha = \pi - \theta'$) and $d\alpha$ be the angle subtended by the radial length $(r_A, r_A + \epsilon)$. The ray BA has the same value of the invariant k , but the integral I changes sign, because its limits are reversed. Thus

$$d\alpha = \frac{\epsilon \tan \alpha}{I r_A (n_A^2 r_A^2 - k^2)^{1/2}}. \quad (\text{A8})$$

We can replace α in terms of θ if we use the ray invariant $k = n_A r_A \sin \theta = n_B r_B \sin \theta'$ for both $\sin \alpha$ and $\cos \alpha$: Use

$$\tan \alpha = \frac{\sin \alpha}{\cos \alpha} = \frac{\sin \theta'}{-\cos \theta'} = \frac{n_A r_A \sin \theta}{-(n_B^2 r_B^2 - k^2)^{1/2}}$$

and

$$(n_A^2 r_A^2 - k^2)^{1/2} = n_A r_A \cos \theta$$

to obtain

$$d\alpha = - \frac{\epsilon \tan \theta}{I r_A (n_B^2 r_B^2 - k^2)^{1/2}}. \quad (\text{A9})$$

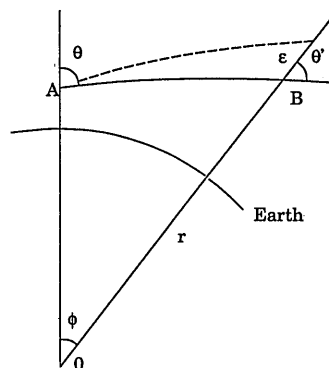


Fig. 9. Rays in a spherically symmetric atmosphere.

Thus the ratio of angles subtended by a short radial distance ϵ is

$$\frac{d\alpha}{d\theta} = \frac{r_B}{r_A}. \quad (\text{A10})$$

This result can be rewritten in terms of angles subtended by short equal-line segments perpendicular to the ray, as

$$\frac{d\alpha}{d\theta} = \frac{n_A}{n_B}. \quad (\text{A11})$$

Thus in general an observer at A looking at an object of height h perpendicular to the ray at B will not see it to the same scale as an observer at B looking at the same object at A.¹⁶

In air, however, n is always close to unity, so this scale difference will scarcely be noticeable.

We can now proceed to the main result. Begin with the case where rays are straight, and consider a small patch δS on the object, of radiance B (see Fig. 10). A lens whose entrance pupil has area δA subtends a solid angle $\delta\Omega$ at δS , where $\delta\Omega = \delta A \cos \eta / l^2$. The lens thus receives radiant power $\delta P = B \cos \xi \delta S \delta\Omega$, which it distributes over the image $\delta S'$ of δS . Let $\delta\omega$ be the solid angle subtended by δS at the lens; this is also the solid angle subtended by the image $\delta S'$ at the lens: $\delta\omega = \delta S \cos \xi / l^2 = \delta S' \cos^3 \eta / f^2$. For straight rays between δS and δA , the solid angle at one end subtended by a unit perpendicular area at the other is the same in both directions, i.e.,

$$\frac{\delta\Omega}{\delta A \cos \eta} = \frac{\delta\omega}{\delta S \cos \xi}. \quad (\text{A12})$$

Image brightness is given by the irradiance at the focal plane (image power per unit area); this quantity is equal to

$$\delta E = \frac{\delta P}{\delta S'} = \frac{B \cos \xi \delta S \delta\Omega}{\delta S'}. \quad (\text{A13})$$

Use Eq. (A12) to eliminate δS and $\delta\Omega$, and then replace $\delta\omega$ to obtain the well-known result for image illumination¹⁷:

$$\delta E = \frac{B \delta A}{f^2} \cos^4 \eta. \quad (\text{A14})$$

We now consider the spherically symmetrical atmo-

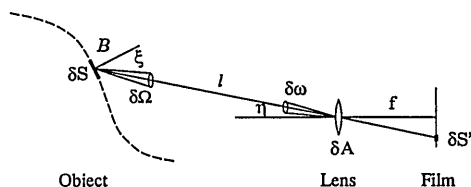


Fig. 10. Straight-ray geometry for calculating image brightness.

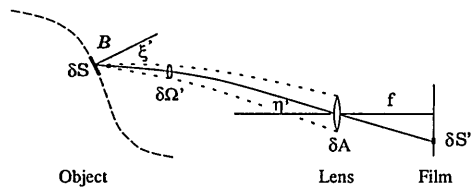


Fig. 11. Curved-ray geometry.

sphere, in which the rays are curved in the vertical plane (see Fig. 11). Since the rays are not deflected laterally, changes in solid angles depend only on vertical deflection. But we showed above that vertical angles subtended by unit lengths normal to the rays were nearly the same (in air) looking both ways along a ray. This implies that Eq. (A12) holds (nearly) for curved rays as well:

$$\frac{\delta\Omega'}{\delta A \cos \eta'} = \frac{\delta\omega'}{\delta S \cos \xi'}. \quad (\text{A15})$$

The image irradiance analysis for this case follows the same steps as for straight rays (above) and produces the same result:

$$\delta E' = \frac{B \delta A}{f^2} \cos^4 \eta'. \quad (\text{A16})$$

For practical mirage images both η and η' are typically $< 1^\circ$; the cosine term is then close to unity for each, and the difference is negligible. Thus the image irradiance in the mirage image [Eq. (A16)] is the same as that for straight rays [Eq. (A14)]. This is intuitively reasonable; in the case of a magnified image, for example, $\delta\omega'$ and $\delta S'$ are, respectively, larger than $\delta\omega$ and δS , but more radiant power is collected from δS to compensate exactly for the increased image area.¹⁸ Thus the relocation of pixel rows in the mirage simulator without changing their brightness is justified, because any spot on a mirage has the same brightness as the corresponding spot on the original.

This study was supported in part by the Natural Sciences and Engineering Research Council of Canada.

References and Notes

1. R. G. Fleagle and J. A. Businger, *An Introduction to Atmospheric Physics*, 2nd ed. (Academic, New York, 1980).
2. W. H. Lehn and R. E. Wallace, "Continuous-tone mirage images computed from digitized source photographs," in *Digest of Topical Meeting on Meteorological Optics* (Optical Society of America, Washington, D.C., 1986), of paper ThB4, pp. 36-38.
3. M. Berger, T. Trout, and N. Levit, "Ray tracing mirages," *IEEE Comput. Graphics Appl.* **10**, 36-41 (1990).
4. A. B. Fraser and W. H. Mach, "Mirages," *Sci. Am.* **234**, 102-111 (1976).
5. W. H. Lehn and M. B. El-Arini, "Computer-graphics analysis of atmospheric refraction," *Appl. Opt.* **17**, 3146-3151 (1978). The TC concept introduced in this reference plots z_{obj} versus ray angle ϕ at the eye. For image calculations it is more

- convenient to interchange the axes and replace ϕ by z_{app} . The latter form previously appeared in J. K. Sparkman, "A remote sensing technique using terrestrial refraction, for the study of low-level lapse rate," Ph.D. dissertation (University of Wisconsin, Madison, Wisconsin, 1971).
6. J. S. Morrish, "Inferior mirages and their corresponding temperature structures," M.Sc. thesis (University of Manitoba, Winnipeg, Canada, 1985).
 7. A. B. Fraser, "Solutions of the refraction and extinction integrals for use in inversions and image formation," *Appl. Opt.* **16**, 160–165 (1977).
 8. W. H. Lehn, "A simple parabolic model for the optics of the atmospheric surface layer," *Appl. Math. Model.* **9**, 447–453 (1985).
 9. W. H. Lehn, "Atmospheric refraction and lake monsters," *Science*, **205**, 183–185 (1979).
 10. W. H. Lehn and I. Schroeder, "The Norse merman as an optical phenomenon," *Nature (London)* **289**, 362–366 (1981).
 11. J. B. Sweeney, *A Pictorial History of Sea Monsters* (Crown, New York, 1972).
 12. F. Bruemmer, *Encounters with Arctic Animals* (McGraw-Hill, Toronto, 1972), p. 73.
 13. L. M. Larson (translator), *The King's Mirror* (Twayne, New York, 1917), pp. 135–136.
 14. W. J. Humphreys, *Physics of the Air*, 3rd ed. (Dover, New York, 1964).
 15. J. M. Pernter and F. Exner, *Meteorologische Optik*, 2nd ed. (Braumüller, Vienna, 1922).
 16. In the case of a flat earth, the ray invariant is $n \sin \theta = k$. Equation (A10) then becomes $d\alpha = d\theta$, but Eq. (A11) remains unchanged.
 17. M. Born and E. Wolf, *Principles of Optics*, 6th ed. (Pergamon, Oxford, 1986).
 18. An unnamed reviewer suggested an alternative approach to this result, based on the discussions of image brightness in Ref. 17: if the atmosphere is regarded as part of the (lossless) image-forming lens, and if the refractive indices of the medium are the same at object and image, the photometric brightness of the image will equal that of the object.